In vitro evaluation of a novel fluoride-coated clear aligner with antibacterial and enamel remineralization abilities

DOI:
10.1007/s00784-023-05216-7

Document Version
Accepted author manuscript

In Vitro Evaluation of a Novel Fluoride-coated Clear Aligner with Antibacterial and Enamel Remineralization Abilities

Jiarong Yan [a,b], *Lingyun Cao* [a,b], *Ting Luo* [a,b], *Danchen Qin* [a,b], *Fang Hua* [a,b,c,*], *Hong He* [a,b,*]

[a.] The State Key Laboratory Breeding Base of Basic Science of Stomatology (Hubei-MOST) & Key Laboratory of Oral Biomedicine Ministry of Education, School & Hospital of Stomatology, Wuhan University, Wuhan, China.

[b.] Department of Orthodontics, School & Hospital of Stomatology, Wuhan University, Wuhan, China

[c.] Division of Dentistry, School of Medical Sciences, Faculty of Biology, Medicine and Health, University of Manchester, Manchester, UK

*** Correspondence**

Assoc. Prof. Fang Hua

School & Hospital of Stomatology, Wuhan University, Luoyu Road 237, Wuhan 430079, China

Email: huafang@whu.edu.cn

Prof. Hong He

School & Hospital of Stomatology, Wuhan University, Luoyu Road 237, Wuhan 430079, China

Email: drhehong@whu.edu.cn

Acknowledgments

This work was supported by the National Natural Science Foundation of China (No. 81901044), and the Chinese Stomatological Association COS Basic Research Fund (No. COS-B2021-08).

Author Contributions

Yan Jiarong: Conceptualization, Methodology, Formal analysis and Writing- Original draft**;** Cao Lingyun: Visualization, Resources**;** Luo Ting: Visualization, Investigation; Qin Danchen: Visualization, Investigation; Hua Fang: Supervision, Conceptualization, Writing - Review & Editing**;** He Hong: Supervision, Conceptualization, Writing - Review & Editing.

In Vitro Evaluation of a Novel Fluoride-coated Clear Aligner with Antibacterial and Enamel Remineralization Abilities

Abstract

Objective:

To investigate the antibacterial and enamel remineralization performances as well as physicochemical properties and biocompatibility of a fluoride-coated clear aligner plastic (FCAP).

Materials and Methods:

FCAP and normal clear aligner plastic (CAP) was bought from the manufacturer (Angelalign Technology Inc, China). The FCAP was observed under scanning electron microscopy. Its element composition, resistance to separation, contact angle and protein adhesion performance were characterized. Colony-forming unit (CFU) count and 3-(4,5)-dimethylthiahiazo (-z-y1)-3,5-di- phenytetrazoliumromide (MTT) assay were used to evaluate the antibacterial ability of *Streptococcus mutans*. Fluoride release-recharge patterns were obtained. Apatite formation was evaluated after immersing FCAP in artificial saliva. Enamel remineralization capability was evaluated in the demineralization model (immersing samples in demineralization solution for 36h) and pH cycling model (immersing samples in demineralization solution and remineralization solution in turns for 14 days). Cell counting kit-8 (CCK-8) and Live/Dead cell staining kits were used for cytotoxicity assay.

Results:

The FCAP showed uniformly distributed fluoride and did not compromise protein adhesion performance. CFU count (5.47±0.55 for CAP, 3.63±0.38 for FCAP) and MTT assay (0.41±0.025 for CAP, 0.28±0.038) indicated that the FCAP had stronger antibacterial activity compared with normal clear aligner plastic (CAP, $P<0.05$ for both evaluations). The FCAP could release fluoride continuously for 14 days and could be recharged after immersing in NaF solution. The FCAP could induce the formation of hydroxyapatite in artificial saliva and could reduce the microhardness decrease, color change and mineral loss of enamels in both two models ($P<0.05$ for all evaluations). CCK-8 and Live/Dead cell staining analyses showed that

the coating did not compromise the biocompatibility of the clear aligner (P>0.05 for CCK-8 evaluation).

Conclusions:

The FCAP had antibacterial, fluoride recharge and enamel remineralization abilities while did not compromise physicochemical properties and biocompatibility.

Clinical Relevance:

The FCAP has the potential to prevent enamel demineralization during clear aligner treatment.

Keywords:

Clear aligner, Fluoride, Antibacterial, Hydroxyapatite, Enamel remineralization

1 Introduction

Orthodontic treatment of malocclusion could not only align and level teeth but also improve the patient's profile [1]. In the last two decades, clear aligners have gradually become popular in orthodontic treatment [2]. Compared with traditional fixed appliances, clear aligner treatment has many advantages, including better comfort, less influence on esthetics, shorter chairside time, and fewer visits [3-8].

It is commonly believed that compared with fixed appliances, clear aligners can facilitate oral hygiene maintenance [9] and thereby reduce the occurrence of enamel demineralization, which is a common side effect of orthodontic treatment [10, 11]. However, studies have found that for patients treated with clear aligners, the oral microbiome was not significantly improved, and no significant decrease in cariogenic bacteria counts was found compared with fixed appliances [12, 13]. Albhaisi and colleagues [14] found that orthodontic patients treated with clear aligners could develop large and shallow white spot lesions (WSLs) during treatment. Therefore, enamel demineralization is still the main concern for clear aligner treatment.

For fixed orthodontic treatment, brackets, wires and adhesives have been experimentally modified to have antimicrobial and/or remineralization abilities [15-18], as alternative strategies to conventional enamel demineralization prevention methods such as mouthwashes and varnishes [19-22]. The modified appliances enable long-term and convenient prevention of enamel demineralization, and the preventive effect relies less on patient compliance. Analogously, for clear aligner treatment, modification of clear aligner material could also be a promising way to prevent enamel demineralization.

Clear aligners control tooth movement through the deformation of plastic [1]. Modification of the plastic material alters its mechanical properties, which may result in unwanted tooth movements. Coating modification can endow aligners with additional properties and minimize the impact on the mechanical properties. Xie and colleagues modified a clear aligner with quaternary ammonium-gold nanoclusters (QA-GNCs) coating, and the QA-GNCs-coated aligner could effectively inhibit the adhesion and growth of cariogenic bacteria [23]. However, no studies have modified clear aligners with a coating that has both antimicrobial and remineralization abilities. The above-mentioned coating aligners are in the laboratory stage and

have not yet been mass-produced and clinically used.

Recently, Angelalign Technology Inc. released a fluorine-coated aligner product which was claimed to have antibacterial and enamel remineralization abilities. Fluoride, a commonly used caries-preventive agent, has antimicrobial and remineralization effects. It inhibits bacterial growth by decreasing bacterial enzyme activity, enhancing the permeability of bacterial cell membranes, increasing proton permeability, and enhancing acid killing and oxidative killing of bacteria [24]. In addition, fluoride could further prevent enamel demineralization by inducing apatite crystallization [25, 26]. Therefore, the fluorine-coated aligner could be a promising orthodontic appliance which has good antimicrobial and enamel remineralization properties to prevent enamel demineralization. However, no studies have been conducted to investigate the antimicrobial and remineralization properties of this fluorine-coated aligner, its performance in preventing enamel demineralization is questionable.

In this study, we investigated the novel multifunctional fluoride-coated clear aligner plastic in vitro. The coating was intended to have good antibacterial, fluoride recharge, apatite formation, and enamel remineralization properties. The null hypotheses were that the fluoride-coated clear aligner did not have 1) antibacterial ability, 2) fluoride rechargeability, 3) apatite formation performance, 4) enamel remineralization ability, and 5) acceptable biocompatibility.

2 Methods and Materials

2.1 The fluoride-coated clear aligner and reference clear aligner

The novel fluoride-coated clear aligner plastic (FCAP, Angelalign, China) and the clear aligner plastic (CAP, Angelalign, China) without any modification were bought from the Angelalign Technology Inc.

2.2 Characterization of the fluoride-coated clear aligner

2.2.1 Scanning electron microscopy observation and element analysis

The CAP and FCAP were carbon-coated (JEE-400, HEOL, Japan) and observed using field emission scanning electron microscopy (FESEM, Zeiss SIGMA, Zeiss, UK) to analyze the surface structure and element composition. To further analyze the distribution of elements, the FCAP was observed under the spectrum analysis mode of a field emission electron probe micro-

analyzer (JXA-8530F Plus, JEOL, Japan).

2.2.2 Resistance to separation assessment

Cross-cut test (referring to ISO-2409:2020, *Paints and varnishes — Cross-cut test*) was used to assess the resistance of the fluoride-containing coating to separation from the clear aligner. A multi-blade cutting tool with 1 mm blade spacing was used to make cuts on the coating side of the FCAP. With uniform pressure on the cutting tool, six cuts were made at a uniform cutting rate breadthways and lengthways. An adhesive tape (#600, 3M, US) was placed fully over the lattices in a direction parallel to the cuts and rubbed with a fingernail to make sufficient contact with the coating. After 5 min, the tape was removed by pulling it off steadily for one second at an angle of 60° with the assistance of a protractor. The cutting area was observed under a stereomicroscope, and the detached cutting area was measured through the Image J software. Three replicates were set. The resistance ability of the coating to separation was divided into the follo wing six classifications:

0: None of the entire cutting areas was detached;

1: Not great than 5% of the cutting area was detached;

2: Greater than 5%, but not greater than 15% of the cutting area was detached;

3: Greater than 15%, but not greater than 35% of the cutting area was detached;

4: Greater than 35%, but not greater than 65% of the cutting area was detached;

5: Greater than 65% of the cutting area was detached;

2.2.3 Protein adhesion measurement

The micro bicinchoninic acid (BCA) method was used to evaluate the protein adhesion performance [27]. The CAP and FCAP were cut into squares of 2.4 cm * 2.4 cm and incubated in phosphate-buffered saline (PBS) at 37 ℃ for 2 h. After incubation, they were transferred into bovine serum albumin (4.5 mg/ml, BSA, Beyotime, China) PBS solution and incubated at 37 ℃ for another 2 h. Squares were then rinsed with PBS on a table concentrator for 5 min. Sodium dodecyl sulfate (SDS, Beyotime, China) was dissolved in PBS to obtain a 1 wt% SDS solution. Each square was immersed in 2 ml SDS solution and sonicated for 20 min to detach all BSA on the square. A BCA protein analysis kit (Beyotime, China) was used to quantify the BSA

concentration in the SDS solution. Briefly, 20 μl of SDS solution and 200 μl of BCA working solution were added into a well of a 96-well plate and incubated at 37 ℃ for 2 h. Then the absorbance of each well at 562 nm was measured using a spectrophotometer (Powerwave 340, Bio-Tek Instrument, US). The absorbance of each square was the average of the three repetitions. A standard curve of BSA concentration – Absorbance was carried out following the manufacturer's instruction to calculate the BSA concentration in the SDS solution. Eight replicates were set for each group**.**

2.2.4 Surface contact angle test

A contact angle system (DSA100S, KRUSS, Germany) was used to measure the contact angle of the CAP and FCAP. One drop of deionized water was dripped on the surface of a sample and the contact angle was measured twice. The average of the two measurements was considered as the contact angle of the sample. Eight replicates were set for each group.

2.3 Antibacterial evaluation

2.3.1 Colony-forming unit assay

The antibacterial evaluation was carried out following ISO standardization (ISO 22196:2007, *Plastics - measurement of antibacterial activity on plastics surface*). The CAP and FCAP were cut into squares of 5.0 cm * 5.0 cm and then sterilized by ultraviolet irradiation for 30 min. *Streptococcus mutans* (*S. mutans*, UA159) were incubated in brain heart infusion (BHI, Sigma, US) broth for 18 h at 37 ℃ micro-aerobically and adjusted to 1×10^6 CFU/ml with BHI broth for further usage. After putting the sample in a sterile culture dish, 0.4 ml of 1×10^6 CFU/mL *S. mutans* solution was dripped on the sample surface and a polypropylene (PP) plastic film of 4.0 cm * 4.0 cm was covered onto the droplet to spread out the *S. mutans* solution to the edge of the PP plastic. The culture dish was incubated at 37 ℃ micro-aerobically for 24 h. After incubation, 10 ml of soya casein digest lecithin polysorbate broth (SCDLP broth, Hopebiol, China) was added to the dish to flush the bacteria off. The SCDLP broth was then diluted by PBS, and BHI solid agar medium (BHI with 1.5 wt% agar) was used to count the number of *S. mutans* colonies. Five replicates were set for each group.

2.3.2 MTT assay

To further evaluate the anti-biofilm ability of the FCAP, the *S. mutans* biofilm was co-cultured with the sample. *S. mutans* were cultured in a sugar-containing BHI medium (BHI with 1 wt% sucrose) for further usage. The sterilized CAP and FCAP were cut into squares of 1.1 cm * 1.1 cm and put into wells of a 24-well plate, and 100 μl of the *S. mutans* solution mentioned above was dripped on the surface of each sample. The 24-well plate was incubated at 37 ℃ micro-aerobically for 24 h. After incubation, 1 mL of 0.5 mg/ml MTT solution (Beyotime, China) was dripped into each well of the 24-well plate to incubate with the biofilm at 37 ℃ micro-aerobically for 1 h. After incubation, the MTT solution was replaced by 1 ml of dimethyl sulfoxide (DMSO, Sigma, US). After shaking the 24-well plate on a table concentrator for 30 min, 200 μl of the DMSO solution from each well was piped into a well of a 96-well plate, and the absorbance of each well at 540 nm was measured using a spectrophotometer (Powerwave 340, Bio-Tek Instrument, US). The absorbance of each sample was the average of three repetitions. Five replicates were set for each group.

2.4 Fluoride rechargeability assessment

The CAP and FCAP were cut into rectangular samples of 2.0 cm * 6.0 cm and immersed in 40 ml deionized water in 50 ml centrifuge tubes. Centrifuge tubes were incubated at 37 ℃, and samples were transferred to new centrifuge tubes every day. After seven days, samples were immersed in a 2×10^4 ppm sodium fluoride (NaF) solution for 30 min to recharge the fluoride. Samples were then transferred to new centrifuge tubes and evaluated for the re-release performance for seven days. Fluorine ion concentration was measured by a fluorine ion concentration meter (Model SA 720, Orion, US). The fluoride released from the FCAP was also measured daily for 14 days. Six replicates were set for each group. The release, recharge, and re-release curves were plotted.

2.5 Apatite formation capacity evaluation

The CAP and FCAP were cut into round pieces of 9.0 cm diameter and put in 90 mm culture dishes. The artificial saliva solution [28-30] was prepared by mixing 130 mM potassium chloride (KCl), 1.5 mM potassium chloride ($CaCl_2$), 0.9 mM monopotassium phosphate (KH_2PO_4), 20 mM 4-(2-hydroxyethyl-)-1-piperazine ethanesulfonic acid (HEPES) and

adjusting pH to 7.0 by 1 mM potassium hydroxide (KOH). The aligner piece was immersed in artificial saliva solution and incubated at 37 ℃ for 1 week. The artificial saliva solution was refreshed every day. After incubation, aligner pieces were carbon-coated and observed using the FESEM. The aligner pieces were also analyzed by an X-ray diffractometer (XRD, XPert Pro, PANalytical B.V, Netherlands). To further determine the elemental composition of the deposit on the FCAP, energy dispersive X-ray analysis (EDX) and element mapping analysis were performed through the FESEM. The deposit was also gathered and evaluated through the XRD to further analyze the crystal texture.

2.6 Enamel remineralization evaluation

2.6.1 Enamel samples preparation

Intact human third molars without caries, restorations, white spot lesions and fractures were collected after getting donors' informed consent. The protocol was approved by the Ethics Committee of School & Hospital of Stomatology, Wuhan University (No. 2017-49). After removing gingival tissues and bone tissues, the molars were stored in 0.1% thymol solution at 4 ℃. Each molar was split into the buccal part and lingual part from the mesiodistal direction using a low-speed saw (IsoMet, Buehler, US), and the roots were excised. Enamel samples were embedded in epoxy resin of 1.0 cm * 1.0 cm * 0.5 cm size with the enamel surface facing upwards, and polished with 600-, 800-, 1000-, 2000- SiC paper (Yuli Abrasive Belts, China) and Al_2O_3 polishing solution in sequence with a polishing time of 1 min respectively. The initial surface microhardness of each sample was measured and samples with a microhardness value >430 or <340 were excluded [31]. Details of the microhardness measure method were described the section 2.6.3. The fifty enamel samples were randomly divided into four groups (n=12), and the rest two samples served as the normal control group for scanning electron microscope observation.

2.6.2 Enamel demineralization process

The CAP and FCAP were cut into rectangular samples of 1.0 cm * 1.0 cm (n=24 for the CAP and n=24 for FCAP samples) and fixed to the enamel surfaces to form the CAP-enamel and FCAP-enamel samples. A circle of double-sided tape (3M9810, 3M, US) was applied around

the plastic to fix it to the epoxy surface, so that there was only a 0.5mm gap between the plastic and the enamel surface. Two enamel demineralization models were used to simulate the demineralized environment in the oral cavity: a pH-cycling model (abbreviated as pH model) and a demineralization solution model (abbreviated as De model). Enamel samples were divided into four groups as follows:

Group-1: CAP-enamel samples in the pH model;

Group-2: FCAP-enamel samples in the pH model;

Group-3: CAP-enamel samples in the De model;

Group-4: FCAP-enamel samples in the De model.

In the pH model, samples were immersed in a demineralization solution (2 mM $CaCl_2$, 2 mM KH_2PO_4, 50 mM acetate, pH 4.5) for 4 h followed by a remineralization solution (1.5 mM $CaCl_2$, 0.9 mM KH_2PO_4, 1 M KOH, 20mM 4-(2-hydroxyethyl)-1-piperazine ethanesulfonic acid, pH 7.0) for 20 h [32, 33]. The pH cycling was performed for 9 days. In the De model, samples were immersed in the demineralization solution (2 mM $CaCl_2$, 2 mM KH_2PO_4, 50 mM acetate, pH 4.5) for 36 h. Solutions were refreshed every day.

2.6.3 Enamel surface microhardness measurement

A Vickers microhardness tester (T1000, Taiming Corporation, China) was used to measure the surface microhardness of enamel samples before and after the demineralization process. For each enamel sample, the microhardness was measured five times with a loading force of 200 gf and a loading time of 10 s to get an average value as the sample's surface microhardness number (SHN). The surface microhardness loss (SHL) was calculated using the following formula (SHN0: before demineralization; SHN1: after demineralization) [34]:

$$\text{SHL}\ (\%) = \left(\frac{\text{SHN0}-\text{SHN1}}{\text{SHN0}}\right) * 100\%$$

2.6.4 Enamel surface color measurement

A spectrophotometer (PR-650 Spectra Scan, Photo Research, US) was used to measure the surface color value of enamel samples before and after the demineralization process. The color value was obtained using the CIE L^*, a^*, b^* color system in which L represents the lightness, a represents the position of the red-green axis and b represents the position of the yellow-blue

axis [35]. For each enamel sample, the color was measured three times before and after the demineralization. And the color change value (ΔE) was calculated using the following formula:

$$\Delta E = ((\Delta L^*)^2 + (\Delta a^*)^2 + (\Delta b^*)^2)^{1/2}$$

2.6.5 Enamel morphology observation and roughness analysis

Before and after the demineralization process, enamel samples were observed under a depth-of-field optical microscope (DFOM, VHX-7000, KEYENCE Corporation, Japan) and three-dimensional structures of enamel surfaces were reconstructed. Under the reconstruction mode, the surface roughness (Sa) of each enamel sample was measured three times in areas of 314 μm^2, and the average value was recorded as the sample's Sa value. The Sa change value (ΔSa) was defined as the difference before and after the demineralization process. To observe the cross-section morphology, two samples of each group were cut across the demineralization area to create the cross-section view and observed under the DFOM.

2.6.6 Enamel microstructure observation and element analysis

Two enamel samples of the four groups and the two normal enamels were dried in a vacuum drying oven for three days and were carbon coated. The surfaces of enamel samples were observed under a scanning electron microscope (SEM, VEGA3, TESCAN, Czech). The elemental composition of the enamel surface was analyzed by the EDX mode of the FESEM and the Ca/P atomic ratio was calculated.

2.6.7 Enamel mineralization evaluation

One enamel sample from the four groups was selected for XRD analysis (X'Pert PRO, PANalytical, Netherlands) to characterize the crystal texture of the enamel surface. Nine enamel samples of each group were subjected to confocal Raman microscope analysis (XploRA Plus, HORIBA Jobin Yvon, French). The scan range was set from 2000 cm^{-1} to 100 cm^{-1} at the wavelength of 785 nm. The peak intensity at 960 cm^{-1} was measured as an indication of enamel mineral content [36]. Each sample's Raman spectrum was obtained three times. Since the two CAP groups (Groups 1 and 3) were found to have reflective layers in the cross-sectional observation of DFOM, one cross-section sample of Group-3 after DFOM observation was analyzed under the Raman intensity mapping mode of the confocal Raman microscope using

960 cm^{-1} as the monitored peak to analyze the subsurface mineral content.

2.7 Cytotoxicity evaluation

2.7.1 Cell Counting Kit-8 assay

The CAP and FCAP were cut into rectangular samples of 2.4 cm * 2.4 cm and co-cultured with 1 ml alpha minimum essential medium (aMEM, Cytiva, US) containing 10% fetal bovine serum (FBS, Gibco, US) at 37 °C with 5% CO_2 atmosphere for 3 days to obtain extracts. Human gingival fibroblasts (HGFs, #2620, ScienCell, US) were seeded in a 96-well plate for 1 *10^4 cells per well and cultured by aMEM with 10% FBS at 37 ℃, 5% CO_2 for further usage. When the cell density reached about 70%, the culture medium was replaced by extracts (100 μL per well, three wells for each extract), and cells with pure culture medium were served as the natural culture group (NC group). After incubating the 96-well plate for 24 h, 10 μL Cell Counting Kit-8 (CCK-8, Beyotime, China) solution was dripped into each well and incubated for another 2 h. The absorbance of each well at 450 nm was measured using a spectrophotometer (Powerwave 340, Bio-Tek Instrument, USA). The absorbance of each extract at 450 nm was the average of three repetitions. Five replicates were set for each group.

2.7.2 Live/dead cell staining analysis

Calcein AM/PI Cell Vitality/Cytotoxicity Assay Kit (Beyotime, China) was used for live/dead cell staining analysis. HGFs were seeded in a 48-well plate for 4 *10^5 cells per well and cultured for further usage. When the cell density reached about 70%, the culture medium was replaced by extracts (400 μL per well), and cells with pure culture medium alone were served as the natural culture group (NC group). After incubating for 24 h, cells were stained by Calcein AM/PI staining solution for 30 min. Fluorescent images were taken by an inverted fluorescence microscope (Eclipse Ti-E, Nikon, Japan). Three replicates were set for each group.

2.8 Statistical analysis

The results of protein adhesion measurement, surface contact angle test, CFU count, MTT assay, SHL analysis, color change measurement, surface roughness change assay, and Raman analysis were shown in mean ± SD and analyzed using an unpaired t-test. Data from the CCK-8 assay were shown in mean ± SD and analyzed using one-way ANOVA followed by Tukey's

multiple comparison tests. The significance level for all tests was set at α=0.05.

3 Results

3.1 Characterizations

FESEM observations showed that both the CAP (Fig 1a) and FCAP (Fig 1b) had smooth surfaces. The elemental composition of the CAP surface was carbon and oxygen (Fig 1a). Fluorine, silicon and nitrogen were detected on the surface of the FCAP (Fig 1b). Element distribution analysis showed a uniform distribution of fluorine on the FCAP (Fig 1b). The coating edges of the cuts (Fig 1c) in three replicates were completely smooth and none of the entire cutting areas was detached. According to the classification of resistance ability, the FCAP was classified as "0", which represented the highest level of resistance to separation. The protein adhesion performance of FCAP was comparable to that of the CAP (0.14±0.0040 for CAP, 0.14±0.0028 for FCAP, P>0.05) (Fig 1d). And the FCAP had a statistically higher contact angle than the CAP (76.74±5.31 for CAP, 82.18±2.13 for FCAP, P<0.05) (Fig 1e).

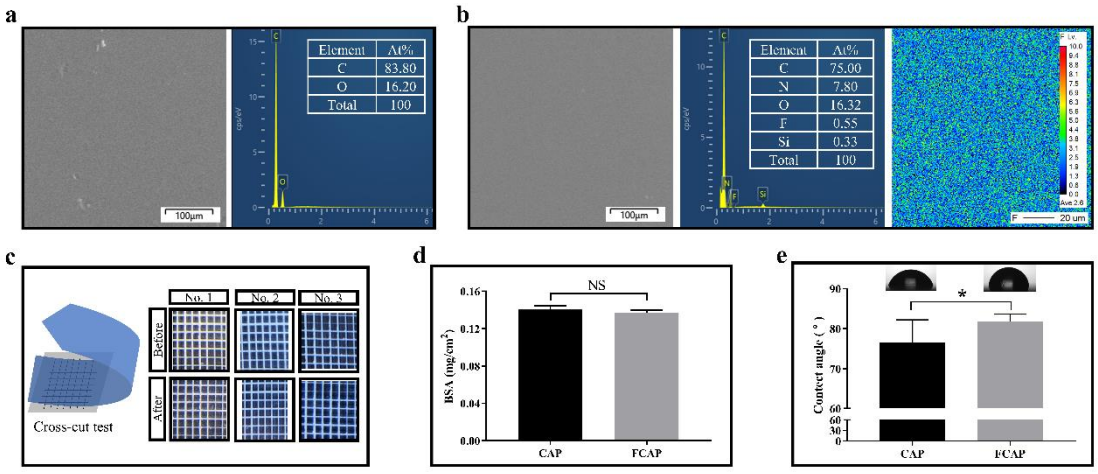

Fig 1 (**a**) FESEM observation showed a smooth surface of the CAP and the elemental composition of the surface was carbon and oxygen; (**b**) The surface of the FCAP was also smooth, and nitrogen, fluorine, and silicon elements appeared in addition to carbon and oxygen. Elemental distribution analysis showed that fluorines were uniformly distributed on the surface of the FCAP; (**c**) Cross-cut assay showed that no coating area was detached in FCAP; (**d**) Protein adhesion analysis showed that the FCAP and CAP had similar protein

(BSA, bovine serum albumin) adhesion performances; (**e**) The FCAP had a significantly larger contact angle than the CAP. NS: No statistical difference, P>0.05; *:P<0.05

3.2 Antibacterial evaluation

Fig 2a shows the schematic of the antibacterial evaluation. Fig 2b shows that the FCAP had a significantly smaller CFU count than the CAP (5.47±0.55 for CAP, 3.63±0.38 for FCAP, P<0.05). Fig 2c shows the schematic of the anti-biofilm evaluation. MTT result showed a similar tendency to the CFU count (Fig 2d), while the FCAP had a significantly smaller absorbance value at 540 nm than the CAP (0.41±0.025 for CAP, 0.28±0.038 for FCAP, P<0.05).

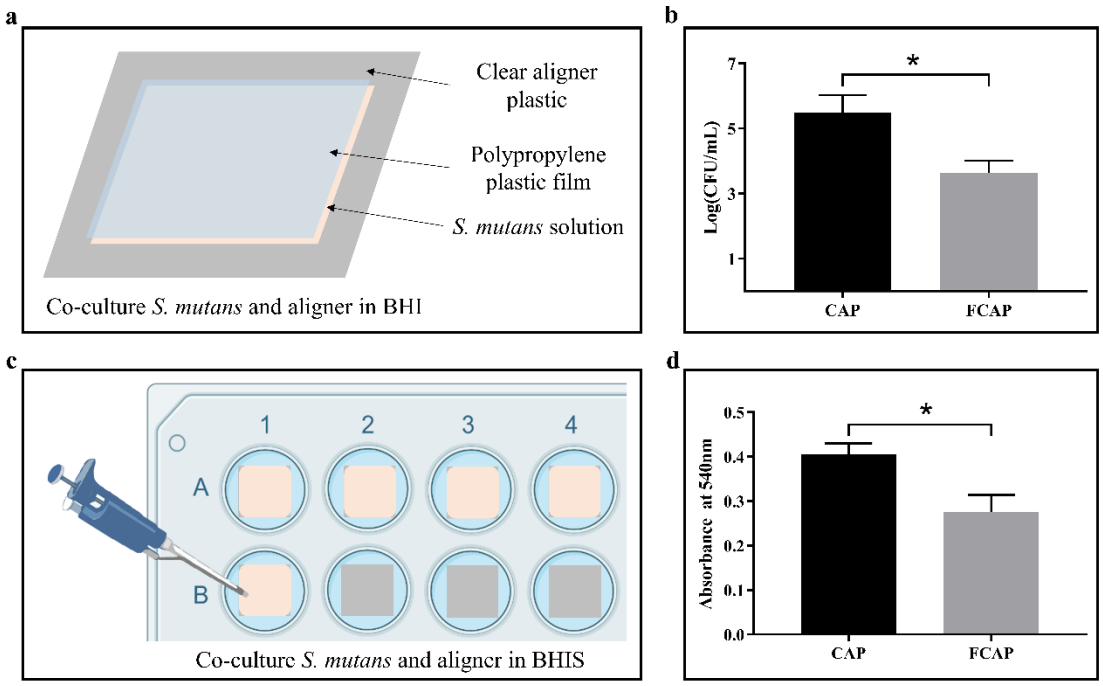

Fig 2 (**a**) Schematic diagram of the colony-forming unit (CFU) assay; (**b**) CFU counts of *S. mutans* showed that the FCAP could reduce the number of *S. mutans* by about two orders of magnitude; (**c**) Schematic diagram of the MTT assay; (**d**) MTT assay showed that the FCAP had a significantly lower absorbance value than CAP. *:P<0.05.

3.3 Fluoride rechargeability

Release, recharge, and re-release curves (Fig 3) showed that the CAP had fluoride release only on the day after recharging (day 8), while the FCAP was able to release fluorine ions continuously for 14 days. After recharging, the re-release of fluorine ions from the FCAP was higher than the baseline level until day 14.

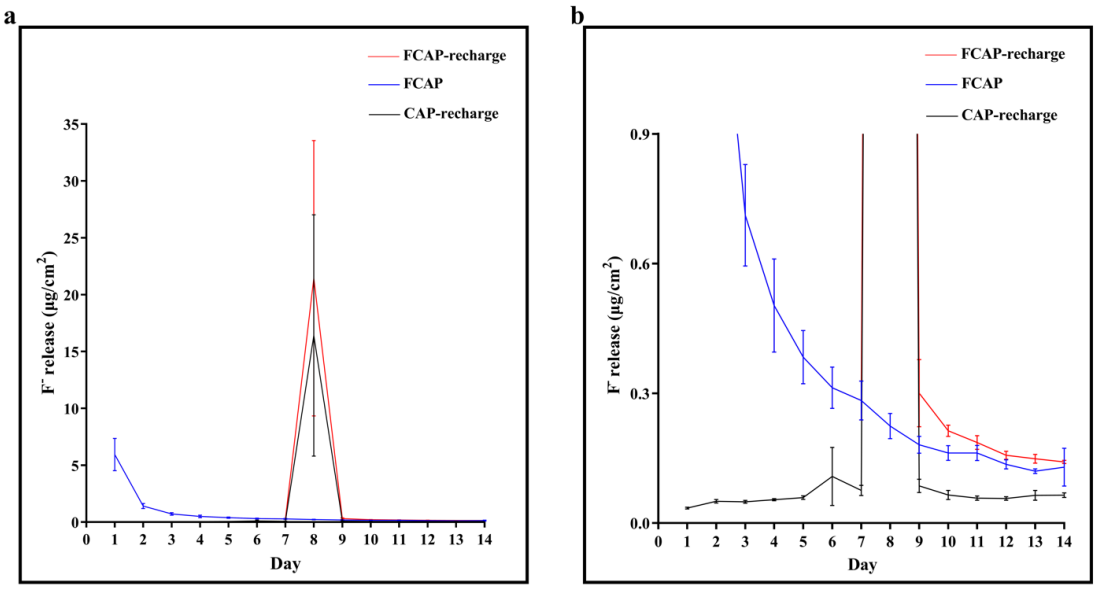

Fig 3 (**a**) Fluoride release and recharge/re-release assessment; (**b**) A partial enlarged view of Figure 3a. The CAP had no fluorine ions released (black line) while the FCAP released fluorine ions continuously for 14 days (blue line). After recharging, the FCAP showed a higher fluoride release amount than its baseline (red line).

3.4 Apatite formation capacity

After being immersed in an artificial saliva solution for one week, the surface of the CAP only had a small count of salt crystals without any apatite-like crystals (Fig 4a). In contrast, the surface of the FCAP was covered with a mineral layer of needle-like crystals that interweaved into a laminar structure and aggregated into spheres in some areas (Fig 4b). EDX analysis showed that in addition to the elements of the aligner itself, elemental peaks of calcium, phosphorus, chlorine, and potassium appeared (Fig 4c). Calcium and phosphorus were uniformly distributed in the mineral layer under element mapping analysis (Fig 4d). XRD pattern of the FCAP had no characteristic peaks (Fig 4e). After being immersed in an artificial saliva solution for one week, the XRD pattern of the FCAP represented some diffraction peaks around 30° to 50° (Fig 4f). And the powder of the mineral layer (Fig 4g) showed similar diffraction peaks compared with the standard XRD pattern of hydroxyapatite (JCPDS 09-0432).

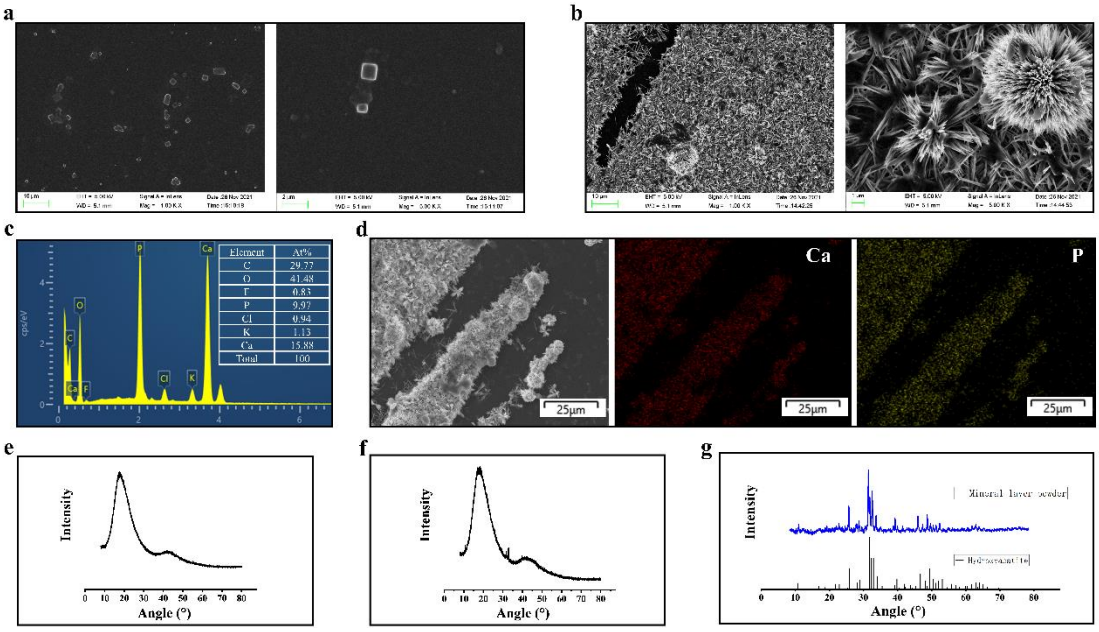

Fig 4 (**a**) The surface of the CAP only had scattered square crystals; (**b**) Interwoven needle-like crystal structures appeared on the surface of the FCAP and aggregated into spherical shapes in some regions; (**c**) EDX analysis showed that the appearance of the mineralized layer made the surface of the FCAP had a large amount of calcium and phosphorus elements; (**d**) Element mapping indicated a uniform distribution of calcium and phosphorus elements within the mineral layer; (**e**) XRD spectrum of the FCAP showed no diffraction peaks; (**f**) XRD spectrum of the FCAP with mineral layer on it had diffraction peaks around 30° to 50°; (**g**) XRD spectrum of the mineral layer powder showed numerous diffraction peaks which corresponded well to the standard diffraction peaks of hydroxyapatite (JCPDS 09-0432).

3.5 Enamel remineralization evaluation

SHL result (Fig 5a) showed that enamel samples of the FCAP groups had significantly smaller SHL values (41.82±17.20 in the De model, 31.67±14.13 in the pH model) than the CAP groups (98.48±0.66 in the De model, 97.74±0.98 in pH model) in both De model and pH model ($P<0.05$ in two models). Compared with CAP groups, the FCAP groups also had significantly fewer color changes (De model: 12.08±3.05 for CAP, 3.43±2.32 for FCAP, $P<0.05$; pH model: 10.02±0.46 for CAP, 7.85±0.75 for FCAP, $P<0.05$) (Fig 5b) and lower enamel surface roughness change (De model: 1.12±0.10 for CAP, 0,81±0.03 for FCAP, $P<0.05$; pH model: 1.04±0.16 for CAP, 0.23±0.14 for FCAP, $P<0.05$) (Fig 5c). DFOM observation (4X) showed

that the colors of enamel samples in the FCAP groups were closer to their original colors, while enamel samples in the CAP groups showed whitish colors (Fig 5d). In addition, the enamel surface of the FCAP group in the pH model had a mineral layer. High magnification (2000X) observation and 3D reconstruction of DFOM showed that in both De and pH models, enamel samples of the CAP groups had rougher surfaces than the FCAP groups (Fig 5d). The results were in accordance with the △Sa result (Fig 5c). The enamel surface of the FCAP group in the pH model showed a different morphology from all other groups, which was observed by the SEM. In the cross-section view, the superficial layers of enamel samples in the two CAP groups both showed whitish structures, while in the FCAP groups, the enamel cross-sections had homogeneous structures (Fig 5d).

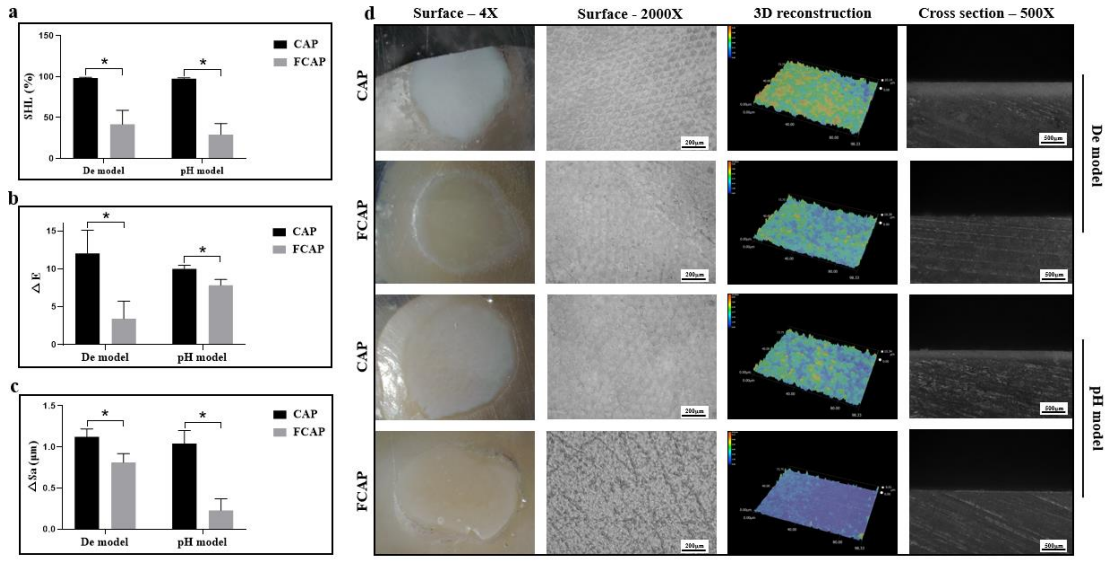

Fig 5 (a) Surface microhardness measurement showed that enamel samples of the FCAP groups in both two models had significantly smaller SHL (%) values than the CAP groups; (**b**) The FCAP groups had significantly fewer color changes (△E) than the CAP groups in the De and pH models; (**c**) The enamel surfaces of the FCAP groups showed significantly lower Sa change (△Sa) than the CAP groups; (**d**) Depth-of-field optical microscope observation showed that enamel samples in the two CAP groups had whiter and rougher surfaces than the FCAP groups respectively; the cross-section views of the CAP groups had layers of structures with different reflectivities, while enamel samples in the FCAP groups showed homogeneous cross-sectional structures. *:P<0.05.

SEM observation further presented the structural differences between groups. Normal enamel had a smooth and flat surface with few scratches (Fig 6). The enamel surface of the CAP group in the De model showed clearly visible prism structures and inter-prism gaps, while the enamel of the FCAP group in the De model had a relatively smooth surface and the prism structures were only faintly visible (Fig 6). In the pH model, the enamel surface of the CAP group also had visible prism structures, while the enamel surface of the FCAP group was covered by a mineral layer with a needle-like structure (Fig 6). EDX analysis showed that both normal enamel and four experimental enamel samples had similar Ca/P atomic ratios of around 1.60 (Fig 6).

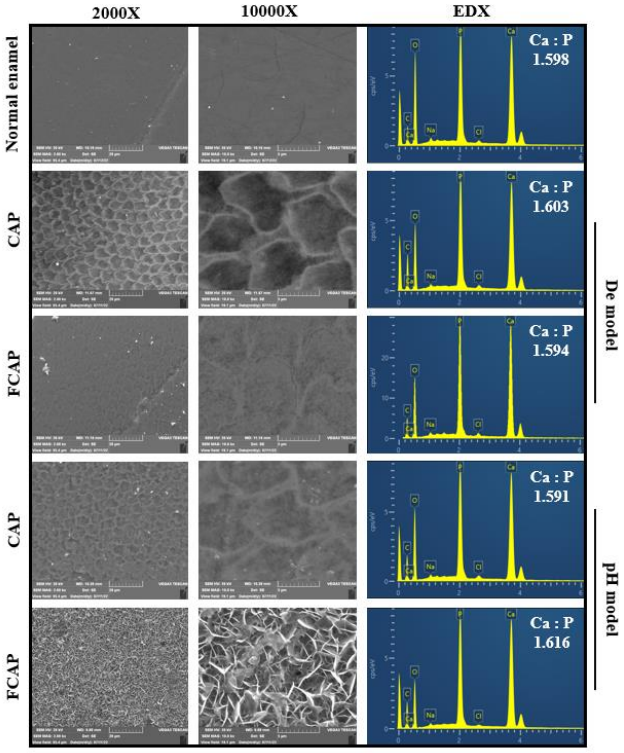

Fig 6 Normal enamel showed a smooth and flat surface while prism structures and inter-prism gaps were visible in the enamel surfaces of the two CAP groups. In the FCAP group of the De model, prism structures were only faintly visible, and in the FCAP group of the pH model, the enamel surface is covered by a layer of needle-like structures. EDX analysis revealed that all four experimental groups had similar Ca/P atomic ratios compared with the normal enamel.

XRD results (Fig 7a) showed that enamel surfaces of all groups had similar diffraction patterns compared with the standard XRD pattern (JCPDS 09-0432) of hydroxyapatite. Fig 7b

shows Raman spectra of enamel surfaces, and four characteristic phosphate peaks around 430, 580, 1040, and 960 cm^{-1} were observed. The 960 cm^{-1} peak had the highest intensity and was used as the indicator of mineral content. In the De model and pH model, enamel samples in the FCAP groups had a stronger peak at 960 cm^{-1} than in the CAP groups. Further quantitative analysis revealed that in both models, enamel samples in the FCAP groups had significantly higher Raman intensity at 960 cm^{-1} than in the CAP groups (De model: 214.71±59.07 for CAP, 538.33±142.18 for FCAP, $P<0.05$; pH model: 265.26±62.85 for CAP, 565.75±252.90 for FCAP, $P<0.05$) (Fig 7c. The Raman intensity mapping at 960 cm^{-1} (Fig 7d) showed that the superficial whitish layer of the enamel in the CAP group of the De model had lower Raman intensity than the deeper enamel which indicated a lower degree of mineralization in the superficial enamel.

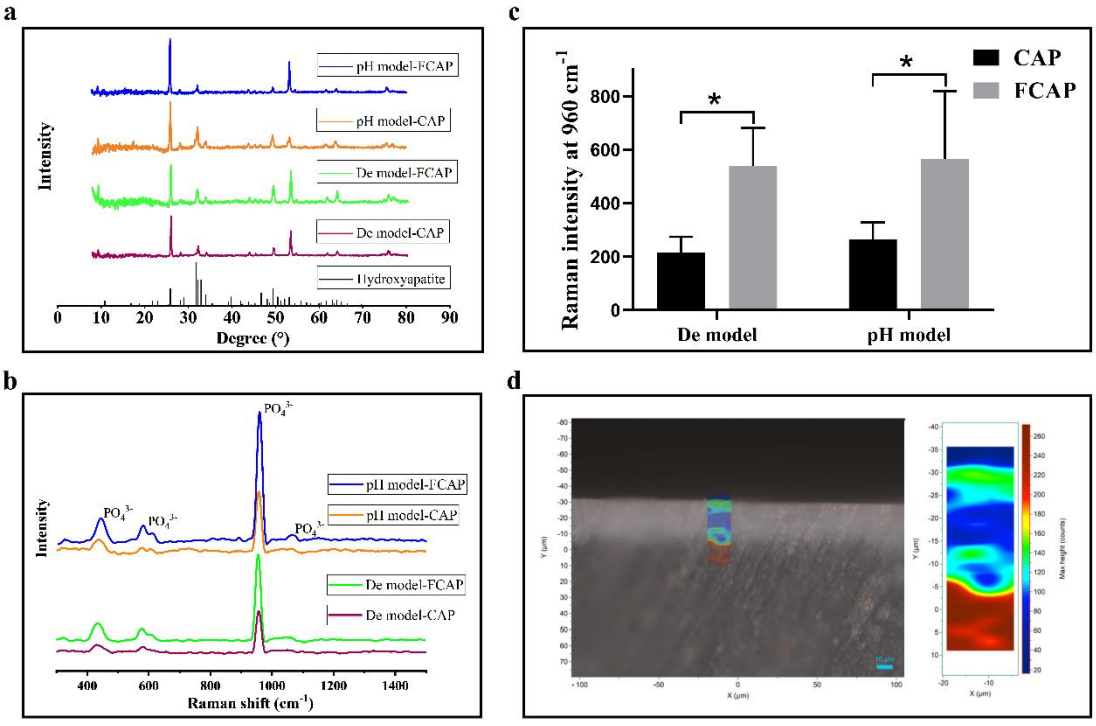

Fig 7 (**a**) XRD spectra of enamel surfaces of all groups had similar diffraction patterns compared with the standard XRD pattern (JCPDS 09-0432) of hydroxyapatite; (**b**) Raman spectra of enamel samples in the CAP and FCAP groups, in which the FCAP groups showed higher Raman intensities at 960 cm^{-1}; (**c**) Quantitative analysis of Raman intensity at 960 cm^{-1} showed that enamel samples of the FCAP groups in two models both had significantly higher Raman intensities than the CAP groups respectively; (**d**) The Raman intensity mapping at 960

cm^{-1} indicated that the cross-section structures with different reflectivities had lower Raman intensities at 960 cm^{-1} than the deeper enamel. *:P<0.05.

3.6 Cytotoxicity

Fig 8a shows the schematic of the cytotoxicity evaluation. CCK-8 assay (Fig 8b) indicated that the absorbance values at 450 nm of the CAP (2.84±0.080) and the FCAP (2.65±0.21) were not statistically different from those of the NC group (2.65±0.24, P>0.05). Live/dead cell staining results (Fig 8c) showed that almost no dead HGFs were visible in all groups.

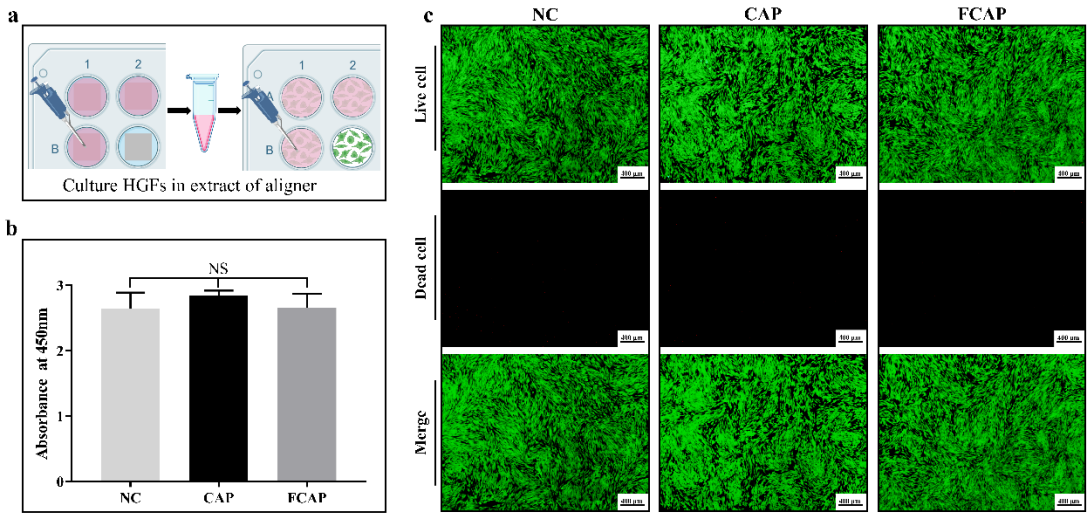

Fig 8 (**a**) Schematic diagram of the cytotoxicity evaluation; (**b**) CCK-8 assay revealed that the absorbance values of CAP and FCAP were similar to those of the NC group; (**c**) Fluorescence microscope observation of live/dead cell staining showed a large amount of green (live) cells and almost no red (dead) cells in all groups. NS: No statistical difference, P>0.05.

4 Discussion

As a newly developed orthodontic technique, the clear aligner is gradually gaining widespread application due to its advantages such as aesthetics, comfort, and ease of cleaning [4, 37-39]. Although clear aligners are good for patients to maintain oral hygiene, enamel demineralization still occurs during clear aligner treatment [14]. In this study, we investigated the antibacterial, fluoride recharge, apatite formation, and enamel remineralization abilities of a fluoride-coated aligner plastic to confirm the enamel remineralization ability before clinical application. Our experiments proved that the FCAP had good antibacterial, fluoride recharge,

apatite formation, and enamel remineralization properties without compromising the biocompatibility of the aligner plastic. Therefore, all five null hypotheses were rejected.

FESEM observation indicated that the coating covered the clear aligner evenly. The elemental composition of the CAP was carbon and oxygen, as well as hydrogen which was undetectable in EDX as hydrogen atoms had only a single layer of electrons [40]. Nitrogen, silicon, and fluorine elements appeared on the surface of the FCAP, which came from the fluoride-containing coating. According to the EDX result, the active ingredient in the coating may be some kind of fluorine-containing silane. Element mapping analysis confirmed the uniform distribution of fluorine in the coating, which meant the coating could achieve a consistent modification effect on the entire aligner surface. The coating had the highest level of resistance to separation so that the coating could remain firmly attached to the surface of the aligner during repeated removing and wearing.

Like any other orthodontic appliance, clear aligners are associated with a worsening oral hygiene status due to the accumulation of food residues and biofilms [41]. Biofilms could deposit on the clear aligner surface and impact oral health [42]. The greater contact angle of the FCAP represented a more hydrophobic surface, making the FCAP more cleanable and having better antifouling properties than the CAP [43, 44]. And the protein adhesion measurement indicated that the presence of the coating did not cause more protein to adhere to the surface of the aligner, which meant no increased biofilm accumulation on the surface of the FCAP [45, 46].

As a common additive to oral health products, fluoride has a good antibacterial property [47-50]. The antibacterial mechanisms of fluoride include 1) inhibiting enzyme activities of bacterial like enolase [51], catalase [52] and phosphatases [53]; 2) penetrating through the membrane to inhibit glycolysis and reducing acid production [24]; 3) enhancing the turnover of cell wall peptidoglycans to induce bacterial lysis [54]; 4) increasing the acid killing and oxidative killing of bacteria[55]. Therefore, we believed that the fluoride-containing coating could endow the aligner with antibacterial ability, and the CFU assay confirmed the excellent antibacterial property of the FCAP. Compared with the CAP, the FCAP could reduce the number of free *S. mutans* by about two orders of magnitude. As cariogenic bacteria could accumulate

into biofilms, we further investigated the anti-biofilm ability of the FCAP. Compared with free bacteria, biofilms are more resistant to antibacterial drugs [56]. MTT assay of anti-biofilm evaluation showed a relatively poor anti-biofilm performance compared to the CFU count results, but the anti-biofilm ability of the FCAP was still significantly enhanced by the fluoride-containing coating. However, the anti-biofilm ability of the FCAP still need to be further confirmed in a more complex biofilm model.

In the present study, samples were immersed in NaF solution for 30 min to be recharged after seven days' release. NaF solution was chosen as the fluoride source because it is a common constituent in mouthwashes and has been used for other fluoride rechargeable materials [57, 58]. The CAP had no fluoride release on all days except for the day after recharging. The fluoride was probably from NaF that had not been washed away completely after immersion. Unlike the CAP, the FCAP showed a continuous fluoride release capacity. After recharging, the FCAP showed significant increases in fluoride release compared to its basal release. The potential mechanism of recharging may be that when the fluoride ions in the coating are released, the silane groups in the coating may be able to take up fluoride ions again in a highly concentrated fluoride ion solution, thus enabling the recharging of fluoride. This rechargeability made the FCAP release more fluorine ions with a single immersion operation, thus providing a better enamel remineralization effect.

The apatite formation ability of the FCAP was evaluated by incubating the aligners with artificial saliva [59]. There were only a few square crystals on the surface of the CAP, which may be salt crystals formed by K^+ and Cl^- in artificial saliva. In contrast, the surface of the FCAP had a mineral layer of interwoven needle-like crystals. The needle-like structure may be attributed to the fluorine ions released from the coating, which could promote crystal growth along the C-axis [59]. EDX analysis revealed that calcium and phosphorus elements appeared in the mineral layer. Element mapping analysis further confirmed that the calcium and phosphorus elements in the mineral layer of the FCAP were uniformly distributed, which meant that the mineral layer consisted of crystals with the same structure and composition. XRD analysis was used to further determine the crystal type of the mineral layer. The XRD pattern of the FCAP had no crystal peaks as the FCAP is an organic polymer. The FCAP with the

mineral layer on it represented some diffraction peaks which indicated that crystals were deposited on the surface. The characteristic diffraction peaks of the mineral layer powder were almost identical to the standard XRD pattern of hydroxyapatite ((JCPDS 09-0432). Combining microstructure observation, elemental analysis, and XRD analysis, we believed that the mineral layer was formed by hydroxyapatite, which confirmed the apatite formation capability of the FCAP.

Fluoride could form fluorapatite and stabilize the hydroxyapatite crystal as fluorapatite has stronger acid resistance [60, 61]. In this study, artificial saliva provided sufficient calcium and phosphorus ions, which co-crystallized with fluorine ions released from the coating to form the fluorapatite [62]. After the initial formation of fluorapatite, they could be the existing apatite seed crystallites of hydroxyapatite to induce the epitaxial deposition of calcium and phosphorus ions [63]. Therefore, the mineral layer on the surface of the FCAP was mainly composed of hydroxyapatite rather than fluorapatite. For the CAP, due to the lack of existing apatite seed crystallites, calcium and phosphorus ions in artificial saliva cannot have epitaxial deposition which results in the absence of the mineral layer [64].

To further explore the enamel remineralization ability of the FCAP, the aligner-enamel samples were treated in two enamel demineralization models and the mineralization of enamel was evaluated. The pH model was used to simulate the pH changes within the oral environment in everyday situations. Samples were cyclically immersed in demineralization (4 h) and remineralization (20 h) solutions for 9 days as each aligner was worn for about one to two weeks [65]. And the De model, which continuously immersed the aligner in the demineralizing solution, was set to simulate the sustained acid attack.

Surface microhardness analysis was used to reflect the degree of enamel mineralization [36]. The SHL results showed that the FCAP could reduce the loss of enamel hardness in both models, thus maintaining the mechanical property of enamel in acid-attacking environments. The *L*a*b** color system was used for quantitative analysis of the enamel color changes before and after demineralization [66]. The FCAP could better maintain the original color of the enamel. In addition, the enamel color in the CAP group of the pH model was less altered compared to the De model, probably because in the pH model, the enamel was able to partially remineralize

in the remineralization solution. In contrast, the FCAP could bring less color change to enamel in the De model compared to the pH model, probably due to the mineral layer that appears on the enamel surface in the pH model. The acid attack leads to the dissolution of enamel, thus making the enamel surface rough. The △Sa result showed that the FCAP could reduce the increase in enamel roughness in the two models. And the FCAP group of the pH model had the lowest roughness change compared to the other three groups, which probably benefited from the mineral layer on the surface of the enamel.

DFOM observation further confirmed the color change and surface roughness change results. Under low magnification, the enamel surfaces of the CAP groups showed white spot lesions-like appearances due to the acid attack, while both the two FCAP groups had more normal enamel appearances. The enamel surface of the FCAP group in the pH model showed a mineral layer that corresponded to the hydroxyapatite formation ability of the FCAP. High magnification observation and 3D reconstruction further confirmed that the FCAP could reduce the demineralization of the enamel. The CAP groups had relatively rougher surfaces than the FCAP groups, and the enamel surface of the FCAP group in the pH model showed a featureless and smooth structure, which was further characterized through SEM observation and XRD analysis. Cross-section views showed that in the two CAP groups, the superficial layers of the enamel had whiter structures that were significantly different from the underlying enamels. We believed that the surface structure with whitish color had less mineral content, and subsequent Raman intensity mapping analysis confirmed our assumption.

SEM observation further demonstrated the difference in enamel structure between the different groups. The normal enamel surface was flat and only had a few scratches caused by polishing. In the two CAP groups, enamel prism imprints and inter-prism gaps were visible, and the enamel from the pH model had a relatively flat surface as the enamel was immersed in the remineralization and demineralization solutions in turns. Compared to the CAP group, the enamel sample of the FCAP group in the De model showed less clear enamel prism imprints and inter-prism gaps, which confirmed the enamel demineralization prevention ability of the FCAP. And the enamel surface of the FCAP group in the pH model had a needle-like mineral layer, which corresponded to the apatite formation results. The XRD spectrogram of the enamel

surface of the FCAP group further indicated that the mineral layer was mostly hydroxyapatite. The EDX analysis showed that the Ca/P atomic ratios of all experimental groups were similar to those of the normal enamel. The Ca/P atomic ratios in all groups were close to but a little bit lower than the Ca/P atomic ratio of hydroxyapatite ($Ca_{10}(PO_4)_6(OH)_2$) which is 1.67. The possible reason was that the hydroxyapatite of enamel was not pure, and other elements like potassium could replace calcium slightly, resulting in the decline of the Ca/P atomic ratio [35].

XRD spectra of all groups showed similar diffraction patterns compared with hydroxyapatite. It meant that after demineralization processes, the enamel surfaces of all groups were still mostly composed of hydroxyapatite. Raman spectra of all groups had four characteristic peaks of phosphate groups at around 960, 430, 1040, and 580 cm^{-1}, which were contributed by asymmetric bending vibration, symmetric bending vibration, asymmetric stretching vibration, and asymmetric stretching vibration of PO_4^{3-}, respectively [36]. Among them, the peak intensity of 960 cm^{-1} represents the content of hydroxyapatite in the enamel and therefore could be used as an indicator of enamel mineral content [67]. Raman intensity analysis indicated that enamels in the two FCAP groups both had significantly more mineral contents respectively which verified the remineralization ability of the FCAP. The Raman intensity mapping result proved that the whitish color structures in the cross-section view of DFOM observation had lower mineral contents than the deeper enamel. Therefore, combining Raman intensity mapping and DFOM observation, we believed that the FCAP could prevent subsurface enamel demineralization.

For biosafety evaluation, according to ISO 10993-5:2009 (*Biological Evaluation of Medical Devices — Part 5: Tests for in vitro cytotoxicity*), we obtained the extracts to assess the in vitro cytotoxicity of the FCAP as the coating only contacts with the enamel. During wear, the coating is most likely to contact indirectly with the gingival tissue through the mediation of saliva. Therefore, gingival fibroblasts were chosen as the experimental subject. After incubation with the extracts, cells in the CAP and FCAP groups all maintained normal morphologies and there were almost no dead cells in both groups. CCK-8 assay further proved the cytocompatibility of the CAP and FCAP. Both the CAP and FCAP had similar absorbance values compared with the

NC group at 450 nm, which indicated all three groups had comparable cell metabolic activities [68].

Our study validated that the fluoride-containing coating could endow the clear aligner with the antibacterial ability so that the FCAP had good inhibitory effects on free cariogenic bacteria and cariogenic biofilms. The FCAP could be recharged by immersing in NaF solution to achieve more fluorine ion release and could induce the formation of hydroxyapatite. Enamel mineralization evaluations after two demineralization processes further confirmed the remineralization ability of the FCAP. The FCAP exhibited good biological safety, supporting its potential for clinical translation. However, there are some limitations of this study that await further exploration. First, although coating modification may minimize the impact on the material itself, the mechanical properties of the FCAP, such as the elasticity modulus, still need to be measured. Second, evaluations of the enamel demineralization prevention property and biocompatibility in more realistic models are needed to better support subsequent clinical translation. In addition, the composition of the coating also needs to be explored to better analyze the mechanism by which it has antibacterial, remineralization and recharging effects.

5 Conclusion

The results of this study indicated that the FCAP had antibacterial, fluoride recharge, apatite formation, and enamel remineralization capabilities with appropriate physicochemical properties and biocompatibility. The modification of the clear aligner with fluoride-containing coating may be a promising strategy for preventing and treating enamel demineralization during clear aligner treatment.

6 Conflict of Interest

The authors declare that they have no conflict of interest.

References

[1] H.W.F.J. William R Proffit, Brent Larson, David M. Sarver (2018) Contemporary orthodontics Sixth ed. Mosby, Saint Louis

[2] T. Weir (2017) Clear aligners in orthodontic treatment. Aust Dent J 62 Suppl 1:58-62. https://doi.org/10.1111/adj.12480

[3] I. Schaefer, B. Braumann, Halitosis (2010) Oral health and quality of life during treatment with Invisalign(®) and the effect of a low-dose chlorhexidine solution. J Orofac Orthop 71:430-441. https://doi.org/10.1007/s00056-010-1040-6

[4] K. Fujiyama, T. Honjo, M. Suzuki, S. Matsuoka, T. Deguchi (2014) Analysis of pain level in cases treated with Invisalign aligner: comparison with fixed edgewise appliance therapy. Prog. Orthod. 15:64. https://doi.org/10.1186/s40510-014-0064-7

[5] M.D. Rosvall, H.W. Fields, J. Ziuchkovski, S.F. Rosenstiel, W.M. Johnston (2009) Attractiveness, acceptability, and value of orthodontic appliances. Am J Orthod Dentofacial Orthop 135:276.e1-12; discussion 276-277. https://doi.org/10.1016/j.ajodo.2008.09.020

[6] P.H. Buschang, S.G. Shaw, M. Ross, D. Crosby, P.M. Campbell (2014) Comparative time efficiency of aligner therapy and conventional edgewise braces. Angle Orthod 84:391-396. https://doi.org/10.2319/062113-466

[7] G. Rossini, S. Parrini, T. Castroflorio, A. Deregibus, C.L. Debernardi (2015) Efficacy of clear aligners in controlling orthodontic tooth movement: a systematic review. Angle Orthod 85:881-889. https://doi.org/10.2319/061614-436.1

[8] D. Fang, F. Li, Y. Zhang, Y. Bai, B.M. Wu (2020) Changes in mechanical properties, surface morphology, structure, and composition of Invisalign material in the oral environment. Am J Orthod Dentofacial Orthop 157:745-753. https://doi.org/10.1016/j.ajodo.2019.05.023

[9] M. Moshiri, J.E. Eckhart, P. McShane, D.S. German (2013) Consequences of poor oral hygiene during aligner therapy. J Clin Orthod 47:494-498

[10] K.C. Julien, P.H. Buschang, P.M. Campbell (2013) Prevalence of white spot lesion formation during orthodontic treatment. Angle Orthod 83:641-647. https://doi.org/10.2319/071712-584.1

[11] A. Lucchese, E. Gherlone (2013) Prevalence of white-spot lesions before and during orthodontic treatment with fixed appliances. Eur J Orthod 35:664-668. https://doi.org/10.1093/ejo/cjs070

[12] Q. Wang, J.B. Ma, B. Wang, X. Zhang, Y.L. Yin, H. Bai (2019) Alterations of the oral microbiome in patients treated with the Invisalign system or with fixed appliances. Am J Orthod Dentofacial Orthop 156:633-640. https://doi.org/10.1016/j.ajodo.2018.11.017

[13] I. Sifakakis, W. Papaioannou, A. Papadimitriou, D. Kloukos, S.N. Papageorgiou, T. Eliades, (2018) Salivary levels of cariogenic bacterial species during orthodontic treatment with thermoplastic aligners or fixed appliances: a prospective cohort study. Prog Orthod 19:25. https://doi.org/10.1186/s40510-018-0230-4

[14] Z. Albhaisi, S.N. Al-Khateeb, E.S. Abu Alhaija (2020) Enamel demineralization during clear aligner orthodontic treatment compared with fixed appliance therapy, evaluated with quantitative light-induced fluorescence: A randomized clinical trial. Am J Orthod Dentofacial Orthop 157:594-601. https://doi.org/10.1016/j.ajodo.2020.01.004

[15] A. Borzabadi-Farahani, E. Borzabadi, E. Lynch (2014) Nanoparticles in orthodontics, a review of antimicrobial and anti-caries applications. Acta Odontol Scand 72:413-417. https://doi.org/10.3109/00016357.2013.859728
[16] J. Bącela, M.B. Łabowska, J. Detyna, A. Zięty, I. Michalak (2020) Functional Coatings for Orthodontic Archwires-A Review. Materials (Basel) 13:3257. https://doi.org/10.3390/ma13153257
[17] Y. Liu, L. Zhang, L.N. Niu, T. Yu, H.H.K. Xu, M.D. Weir, T.W. Oates, F.R. Tay, J.H. Chen (2018) Antibacterial and remineralizing orthodontic adhesive containing quaternary ammonium resin monomer and amorphous calcium phosphate nanoparticles. J Dent 72:53-63. https://doi.org/10.1016/j.jdent.2018.03.004
[18] F. Yu, Y. Dong, H.H. Yu, P.T. Lin, L. Zhang, X. Sun, Y. Liu, Y.N. Xia, L. Huang, J.H. Chen, (2017) Antibacterial Activity and Bonding Ability of an Orthodontic Adhesive Containing the Antibacterial Monomer 2-Methacryloxylethyl Hexadecyl Methyl Ammonium Bromide. Sci Rep 7:41787. https://doi.org/10.1038/srep41787
[19] A. Ali, H. Ismail, K. Amin (2022) Effect of nanosilver mouthwash on prevention of white spot lesions in patients undergoing fixed orthodontic treatment - a randomized double-blind clinical trial. J Dent Sci 17:249-255. https://doi.org/10.1016/j.jds.2021.03.016
[20] T.R. Bauer Faria, V.F. Furletti-Goes, C.M. Franzini, A.A. de Aro, T.A.M. de Andrade, A. Sartoratto, C.C. de Menezes (2021) Anti-inflammatory and antimicrobial effects of Zingiber officinale mouthwash on patients with fixed orthodontic appliances. Am J Orthod Dentofacial Orthop 159:21-29. https://doi.org/10.1016/j.ajodo.2019.10.025
[21] L.N. Flynn, K. Julien, A. Noureldin, P.H. Buschang (2022) The efficacy of fluoride varnish vs a filled resin sealant for preventing white spot lesions during orthodontic treatment. Angle Orthod 92:204-212. https://doi.org/10.2319/052521-418.1
[22] P. Poornima, J. Krithikadatta, R.R. Ponraj, N. Velmurugan, A. Kishen (2021) Biofilm formation following chitosan-based varnish or chlorhexidine-fluoride varnish application in patients undergoing fixed orthodontic treatment: a double blinded randomised controlled trial. BMC Oral Health 21:465. https://doi.org/10.1186/s12903-021-01805-8
[23] Y. Xie, M. Zhang, W. Zhang, X. Liu, W. Zheng, X. Jiang (2020) Gold Nanoclusters-Coated Orthodontic Devices Can Inhibit the Formation of Streptococcus mutans Biofilm. ACS Biomater Sci Eng 6:1239-1246. https://doi.org/10.1021/acsbiomaterials.9b01647
[24] R.E. Marquis (1995) Antimicrobial actions of fluoride for oral bacteria. Can J Microbiol 41:955-964. https://doi.org/10.1139/m95-133
[25] K. Rošin-Grget, K. Peroš, I. Sutej, K (2013) Bašić, The cariostatic mechanisms of fluoride. Acta Med Acad 42:179-188. https://doi.org/10.5644/ama2006-124.85
[26] H.C. Margolis, E.C. Moreno (1990) Physicochemical perspectives on the cariostatic mechanisms of systemic and topical fluorides. J Dent Res 69:606-613; discussion:634-636. https://doi.org/10.1177/00220345900690S119
[27] N. Zhang, M.A. Melo, C. Chen, J. Liu, M.D. Weir, Y. Bai, H.H. Xu (2015) Development of a multifunctional adhesive system for prevention of root caries and secondary caries. Dent Mater 31:1119-1131. https://doi.org/10.1016/j.dental.2015.06.010
[28] Y. Kim, H.H. Son, K. Yi, J.S. Ahn, J. Chang (2016) Bleaching Effects on Color, Chemical, and Mechanical Properties of White Spot Lesions. Oper Dent 41: 318-326. https://doi.org/10.2341/15-015-L

[29] Y. Kim, H.H. Son, K. Yi, H.Y. Kim, J. Ahn, J. Chang (2013) The color change in artificial white spot lesions measured using a spectroradiometer. Clin Oral Investig 17:139-146. https://doi.org/10.1007/s00784-012-0680-x
[30] E.E. Jansen, H. Meyer-Lueckel, M. Esteves-Oliveira, R.J. Wierichs (2021) Do bleaching gels affect the stability of the masking and caries-arresting effects of caries infiltration-in vitro. Clin Oral Investig 25:4011-4021. https://doi.org/10.1007/s00784-020-03732-4
[31] F. Hua, J. Yan, S. Zhao, H. Yang, H. He (2020) In vitro remineralization of enamel white spot lesions with a carrier-based amorphous calcium phosphate delivery system, Clin Oral Investig 24:2079-2089. https://doi.org/10.1007/s00784-019-03073-x
[32] J.Y. Niu, I.X. Yin, W.K.K. Wu, Q.L. Li, M.L. Mei, C.H. Chu (2021) A novel dual-action antimicrobial peptide for caries management. J Dent 111:103729. https://doi.org/10.1016/j.jdent.2021.103729
[33] N. Kohda, M. Iijima, K. Kawaguchi, H. Toshima, T. Muguruma, K. Endo, I. Mizoguchi (2015) Inhibition of enamel demineralization and bond-strength properties of bioactive glass containing 4-META/MMA-TBB-based resin adhesive. Eur J Oral Sci 123:202-207. https://doi.org/10.1111/eos.12187
[34] Y. Zhu, J. Yan, B.M. Mujtaba, Y. Li, H. Wei, S. Huang (2021) The dual anti-caries effect of carboxymethyl chitosan nanogel loaded with chimeric lysin ClyR and amorphous calcium phosphate. Eur J Oral Sci 129:e12784. https://doi.org/10.1111/eos.12784
[35] F. Hua, J. Yan, S. Zhao, H. Yang, H. He (2019) In vitro remineralization of enamel white spot lesions with a carrier-based amorphous calcium phosphate delivery system. Clin Oral Investig 24:2079-2089. https://doi.org/10.1007/s00784-019-03073-x
[36] J. Zhang, V. Boyes, F. Festy, R.J.M. Lynch, T.F. Watson, A. Banerjee (2018) In-vitro subsurface remineralisation of artificial enamel white spot lesions pre-treated with chitosan. Dent Mater 34:1154-1167. https://doi.org/10.1016/j.dental.2018.04.010
[37] A. Azaripour, J. Weusmann, B. Mahmoodi, D. Peppas, A. Gerhold-Ay, C.J. Van Noorden, B. Willershausen (2015) Braces versus Invisalign®: gingival parameters and patients' satisfaction during treatment: a cross-sectional study. BMC Oral Health 15:69. https://doi.org/10.1186/s12903-015-0060-4
[38] C. Flores-Mir, J. Brandelli, C. Pacheco-Pereira (2018) Patient satisfaction and quality of life status after 2 treatment modalities: Invisalign and conventional fixed appliances. Am J Orthod Dentofacial Orthop 154:639-644. https://doi.org/10.1016/j.ajodo.2018.01.013
[39] G.M. Abbate, M.P. Caria, P. Montanari, C. Mannu, G. Orrù, A. Caprioglio, L. Levrini (2015) Periodontal health in teenagers treated with removable aligners and fixed orthodontic appliances. J Orofac Orthop 76:240-250. https://doi.org/10.1007/s00056-015-0285-5
[40] Kotz JC, Treichel PM, Moran MJ (2011) Chemistry And Chemical Reactivity 8th ed. CENGAGE Learning, Boston
[41] L. Lombardo, M. Martini, F. Cervinara, G.A. Spedicato, T. Oliverio, G. Siciliani (2017) Comparative SEM analysis of nine F22 aligner cleaning strategies. Prog Orthod 18:26. https://doi.org/10.1186/s40510-017-0178-9
[42] D. Steinberg, S. Eyal (2004) Initial biofilm formation of Streptococcus sobrinus on various orthodontics appliances. J Oral Rehabil 31:1041-1045. https://doi.org/10.1111/j.1365-2842.2004.01350.x

[43] A.C. Ambarita, S. Mulyati, N. Arahman, M.R. Bilad, N. Shamsuddin, N.M. Ismail (2021) Improvement of Properties and Performances of Polyethersulfone Ultrafiltration Membrane by Blending with Bio-Based Dragonbloodin Resin. Polymers (Basel) 13:4436. https://doi.org/10.3390/polym13244436
[44] J.E. Lee, H.K. Kim (2019) Self-cleanable, waterproof, transparent, and flexible Ag networks covered by hydrophobic polytetrafluoroethylene for multi-functional flexible thin film heaters. Sci Rep 9:16723. https://doi.org/10.1038/s41598-019-53243-w
[45] F. Sun, H.C. Hung, W. Yan, K. Wu, A.A. Shimchuk, S.D. Gray, W. He, X. Huang, H. Zhang (2021) Inhibition of oral biofilm formation by zwitterionic nonfouling coating. J Biomed Mater Res B Appl Biomater 109:1418-25. https://doi.org/10.1002/jbm.b.34801
[46] D.G. Moussa, W.L. Siqueira (2021) Bioinspired caries preventive strategy via customizable pellicles of saliva-derived protein/peptide constructs. Sci Rep 11:17007. https://doi.org/10.1038/s41598-021-96622-y
[47] X. Chen, S. Zhao, S. Chu, S. Liu, M. Yu, J. Li, F. Gao, Y. Liu (2022) A novel sustained release fluoride strip based Poly(propylene carbonate) for preventing caries. Eur J Pharm Sci 171:106128. https://doi.org/10.1016/j.ejps.2022.106128
[48] C. Qi, X. Peng, S. Yuan, M. Zhang, X. Xu, X. Cheng (2022) Evaluation of the Antibacterial and Anti-Inflammatory Effects of a Natural Products-Containing Toothpaste. Front Cell Infect Microbiol 12:827643. https://doi.org/10.3389/fcimb.2022.827643
[49] P.K. Sreenivasan, V.I. Haraszthy, C.C. Rayela, 2021. Antimicrobial effects in oral microenvironments by a novel herbal toothpaste, Contemp. Clin. Trials. Commun. 21, 100680. https://doi.org/10.1016/j.conctc.2020.100680
[50] N.B. Arweiler, F. Müller-Breitenkamp, C. Heumann, O. Laugisch, T.M. Auschill, Antibacterial Action (2021) Substantivity and Anti-plaque Effect of Different Toothpaste Slurries - A Randomised Controlled Trial. Oral Health Prev Dent 19:529-536. https://doi.org/10.3290/j.ohpd.b2182977
[51] L. Lebioda, E. Zhang, K. Lewinski, J.M. Brewer (1993) Fluoride inhibition of yeast enolase: crystal structure of the enolase-Mg(2+)-F(-)-Pi complex at 2.6 A resolution. Proteins 16:219-225. https://doi.org/10.1002/prot.340160302
[52] E.A. Thibodeau, T.F. Keefe (1990) pH-dependent fluoride inhibition of catalase activity, Oral Microbiol Immunol 5:328-331. https://doi.org/10.1111/j.1399-302x.1990.tb00435.x
[53] A.A. Baykov, E.B. Dubnova, N.P. Bakuleva, O.A. Evtushenko, R.G. Zhen, P.A. Rea (1993) Differential sensitivity of membrane-associated pyrophosphatases to inhibition by diphosphonates and fluoride delineates two classes of enzyme. FEBS Lett 327:199-202. https://doi.org/10.1016/0014-5793(93)80169-u
[54] E.A. Thibodeau, C.M. Ford (1991) Chain formation and de-chaining in Streptococcus sobrinus SL-1. Oral Microbiol Immunol 6:313-315. https://doi.org/10.1111/j.1399-302x.1991.tb00500.x
[55] W.A. Belli, D.H. Buckley, R.E. Marquis (1995) Weak acid effects and fluoride inhibition of glycolysis by Streptococcus mutans GS-5. Can J Microbiol 41:785-791. https://doi.org/10.1139/m95-108
[56] I. Ahamad, F. Bano, R. Anwer, P. Srivastava, R. Kumar, T. Fatma (2021) Antibiofilm Activities of Biogenic Silver Nanoparticles Against Candida albicans. Front Microbiol 12:741493. https://doi.org/10.3389/fmicb.2021.741493

[57] L. Zhang, M.D. Weir, L.C. Chow, J.M. Antonucci, J. Chen, H.H. Xu (2016) Novel rechargeable calcium phosphate dental nanocomposite. Dent Mater 32:285-293. https://doi.org/10.1016/j.dental.2015.11.015
[58] J. Yi, M.D. Weir, M.A.S. Melo, T. Li, C.D. Lynch, T.W. Oates, Q. Dai, Z. Zhao, H.H.K. Xu (2019) Novel rechargeable nano-CaF(2) orthodontic cement with high levels of long-term fluoride release. J Dent 90:103214. https://doi.org/10.1016/j.jdent.2019.103214
[59] N.A. Al-Eesa, A. Johal, R.G. Hill, F.S.L. Wong (2018) Fluoride containing bioactive glass composite for orthodontic adhesives - Apatite formation properties. Dent Mater 34:1127-1133. https://doi.org/10.1016/j.dental.2018.04.009
[60] T. Tanaka, T. Kobayashi, Y. Tamenori, A. Sakanaka, T. Kuriki, A. Amano (2019) Phosphoryl oligosaccharides of calcium enhance mineral availability and fluorapatite formation. Arch Oral Biol 101:135-141. https://doi.org/10.1016/j.archoralbio.2019.03.018
[61] E. Jay, M. Rushton, R. Grimes (2012) Migration of fluorine in fluorapatite - A concerted mechanism. J Mater Chem 22:6097-6103. https://doi.org/10.1039/c2jm16235k
[62] K. Pajor, L. Pajchel, J. Kolmas (2019) Hydroxyapatite and Fluorapatite in Conservative Dentistry and Oral Implantology-A Review. Materials (Basel) 12:2683. https://doi.org/10.3390/ma12172683
[63] R. Ramadoss, R. Padmanaban, B. Subramanian (2022) Role of bioglass in enamel remineralization: Existing strategies and future prospects-A narrative review. J Biomed Mater Res B Appl Biomater 110:45-66. https://doi.org/10.1002/jbm.b.34904
[64] M.K. Arifa, R. Ephraim, T. Rajamani (2019) Recent Advances in Dental Hard Tissue Remineralization: A Review of Literature. Int J Clin Pediatr Dent 12:139-144. https://doi.org/10.5005/jp-journals-10005-1603
[65] M. Al-Nadawi, N.D. Kravitz, I. Hansa, L. Makki, D.J. Ferguson, N.R. Vaid (2021) Effect of clear aligner wear protocol on the efficacy of tooth movement. Angle Orthod 91:157-163. https://doi.org/10.2319/071520-630.1
[66] N.A.N. Júnior, G.P. Nunes, A.S. Gruba, M. Danelon, L. da Silva, G. de Farias Batista, A.L.F. Briso, A.C.B. Delbem (2022) Evaluation of bleaching efficacy, microhardness, and trans-amelodentinal diffusion of a novel bleaching agent for an in-office technique containing hexametaphosphate and fluoride. Clin Oral Investig 26:5071-5078. https://doi.org/10.1007/s00784-022-04480-3
[67] B. Mohanty, D. Dadlani, D. Mahoney, A.B. Mann (2013) Characterizing and identifying incipient carious lesions in dental enamel using micro-Raman spectroscopy. Caries Res 47:27-33. https://doi.org/10.1159/000342432
[68] Y. Xu, A.B. Xepapadeas, B. Koos, J. Geis-Gerstorfer, P. Li, S. Spintzyk (2021) Effect of post-rinsing time on the mechanical strength and cytotoxicity of a 3D printed orthodontic splint material. Dent Mater 37:e314-327. https://doi.org/10.1016/j.dental.2021.01.016

Figure captions

Fig 1 (**a**) FESEM observation showed a smooth surface of the CAP and the elemental composition of the surface was carbon and oxygen; (**b**) The surface of the FCAP was also smooth, and nitrogen, fluorine, and silicon elements appeared in addition to carbon and oxygen. Elemental distribution analysis showed that fluorines were uniformly distributed on the surface of the FCAP; (**c**) Cross-cut assay showed that no coating area was detached in FCAP; (**d**) Protein adhesion analysis showed that the FCAP and CAP had similar protein (BSA, bovine serum albumin) adhesion performances; (**e**) The FCAP had a significantly larger contact angle than the CAP. NS: No statistical difference, $P>0.05$; *:$P<0.05$.

Fig 2 (**a**) Schematic diagram of the colony-forming unit (CFU) assay; (**b**) CFU counts of *S. mutans* showed that the FCAP could reduce the number of *S. mutans* by about two orders of magnitude; (**c**) Schematic diagram of the MTT assay; (**d**) MTT assay showed that the FCAP had a significantly lower absorbance value than CAP. *:$P<0.05$.

Fig 3 (**a**) Fluoride release and recharge/re-release assessment; (**b**) A partial enlarged view of Figure 3a. The CAP had no fluorine ions released (black line) while the FCAP released fluorine ions continuously for 14 days (blue line). After recharging, the FCAP showed a higher fluoride release amount than its baseline (red line).

Fig 4 (**a**) The surface of the CAP only had scattered square crystals; (**b**) Interwoven needle-like crystal structures appeared on the surface of the FCAP and aggregated into spherical shapes in some regions; (**c**) EDX analysis showed that the appearance of the mineralized layer made the surface of the FCAP had a large amount of calcium and phosphorus elements; (**d**) Element mapping indicated a uniform distribution of calcium and phosphorus elements within the mineral layer; (**e**) XRD spectrum of the FCAP showed no diffraction peaks; (**f**) XRD spectrum of the FCAP with mineral layer on it had diffraction peaks around 30° to 50°; (**g**) XRD spectrum of the mineral layer powder showed numerous diffraction peaks which corresponded well to the standard diffraction peaks of hydroxyapatite (JCPDS 09-0432).

Fig 5 (a) Surface microhardness measurement showed that enamel samples of the FCAP groups in both two models had significantly smaller SHL (%) values than the CAP groups; (**b**) The FCAP groups had significantly fewer color changes (△E) than the CAP groups in the De and pH models; (**c**) The enamel surfaces of the FCAP groups showed significantly lower Sa change (△Sa) than the CAP groups; (**d**) Depth-of-field optical microscope observation showed that enamel samples in the two CAP groups had whiter and rougher surfaces than the FCAP groups respectively; the cross-section views of the CAP groups had layers of structures with different reflectivities, while enamel samples in the FCAP groups showed homogeneous cross-sectional structures. *:$P<0.05$.

Fig 6 Normal enamel showed a smooth and flat surface while prism structures and inter-prism gaps were visible in the enamel surfaces of the two CAP groups. In the FCAP group of the De model, prism structures were only faintly visible, and in the FCAP group of the pH model, the enamel surface is covered by a layer of needle-like structures. EDX analysis revealed that all four experimental groups had similar Ca/P atomic ratios compared with the normal enamel.

Fig 7 (**a**) XRD spectra of enamel surfaces of all groups had similar diffraction patterns compared with the standard XRD pattern (JCPDS 09-0432) of hydroxyapatite; (**b**) Raman spectra of enamel samples in the CAP and FCAP groups, in which the FCAP groups showed higher Raman intensities at 960 cm^{-1}; (**c**) Quantitative analysis of Raman intensity at 960 cm^{-1} showed that enamel samples of the FCAP groups in two models both had significantly higher Raman intensities than the CAP groups respectively; (**d**) The Raman intensity mapping at 960 cm^{-1} indicated that the cross-section structures with different reflectivities had lower Raman intensities at 960 cm^{-1} than the deeper enamel. *:$P<0.05$.

Fig 8 (**a**) Schematic diagram of the cytotoxicity evaluation; (**b**) CCK-8 assay revealed that the absorbance values of CAP and FCAP were similar to those of the NC group; (**c**) Fluorescence microscope observation of live/dead cell staining showed a large amount of green (live) cells and almost no red (dead) cells in all groups. NS: No statistical difference, $P>0.05$.